Vaporisation and Thermal Decomposition of Dialkylimidazolium Halide Ion Ionic Liquids

K. R. J. Lovelock[#]*, J. P. Armstrong, P. Licence, R. G. Jones

Affiliations:
School of Chemistry, The University of Nottingham, University Park, Nottingham, NG7 2RD, U.K.
Current Address: [#] Department of Chemistry, Imperial College London, London, SW7 2AZ, U.K.

* Correspondence to: kevin.lovelock@imperial.ac.uk

1. Dipping

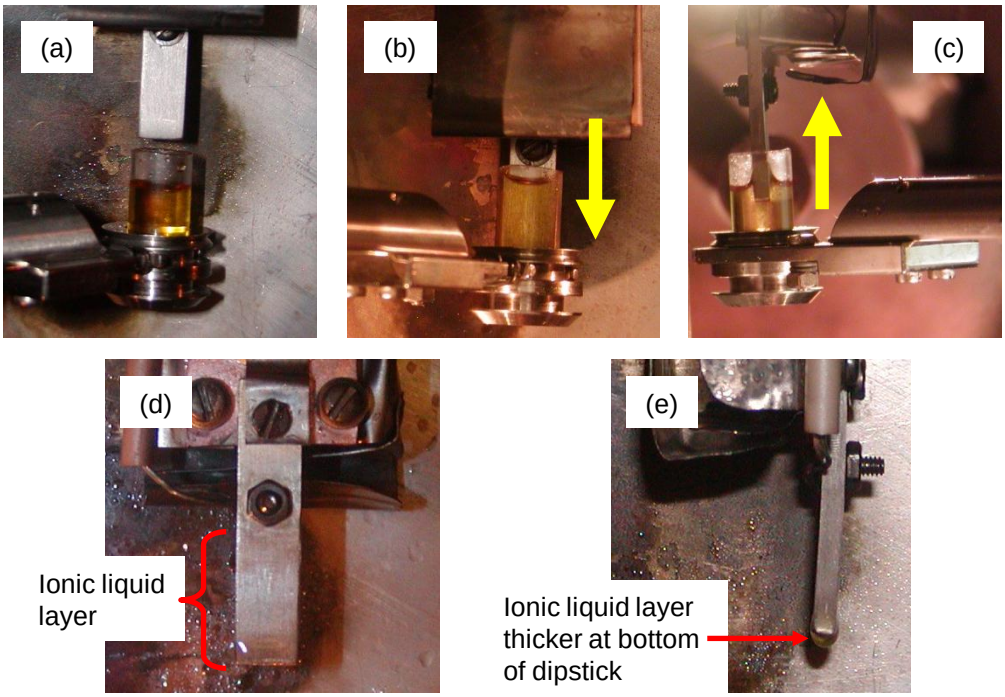

Figure S1. Creating a thin ionic liquid film using the transfer arm. The ionic liquid is $[C_8C_1Im]I$. (a) Before dipping. (b) Dipstick fully immersed in ionic liquid. (c) Withdrawing dipstick from the ionic liquid. Notice the ionic liquid pulling the meniscus of the ionic liquid due to the surface tension. (d) After dipping (front view). (e) After dipping (side view).

To obtain a thin ionic liquid film the polycrystalline silver dipstick was dipped approximately 10 mm into the glass vial containing the ionic liquid. All ionic liquids studied were sufficiently viscous that the upright dipstick method could be used. Figure S1 shows the dipping process for the ionic liquid $[C_8C_1Im]I$. Figure S1a was taken before dipping, Figure S1b was taken when the dipstick has been fully lowered into the ionic liquid. Figure S1c was when the dipstick was being removed from the ionic liquid; notice how the particularly viscous $[C_8C_1Im]I$ clings to the dipstick. Figure S1c also suggests that the Wilhelmy plate method for measuring surface tension at UHV is a viable option for ionic liquids. Figures S1d and S1e show the dipstick when covered with a thin film of ionic liquid. For more viscous ionic liquids the layer was generally thicker; this difference can be seen in Figure S2 as the "bulb" at the base of the dipstick was much larger for $[C_8C_1Im]I$ than for $[C_4C_1Pyrr][Tf_2N]$.

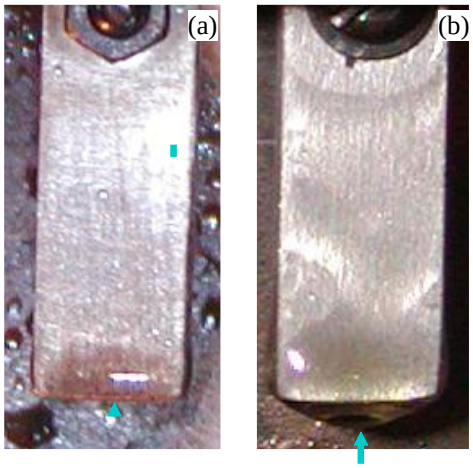

Figure S2. The amount of ionic liquid on the dipstick immediately after dipping at room temperature. The amount was dependent upon the viscosity of the ionic liquid. (a) $[C_4C_1Pyrr][Tf_2N]$. (b) $[C_8C_1Im]I$.

It was serendipitous that for most of the ionic liquids studied using LOSMS to date the maximum chamber pressure value during desorption experiments was ~2×10^{-7} mbar, well below the maximum operating pressure of the mass spectrometer channeltron of 5×10^{-6} mbar. An example of the chamber pressure change that occurred during desorption of $[C_2C_1Im][C_2OSO_3]$ is shown in Figure S3a. An example of the chamber pressure change that occurred during desorption of $[C_8C_1Im]Cl$ is shown in Figure S3b. The maximum operating pressure of the channeltron was reached and consequently had to be turned off. Therefore, the high temperature cut-off could not be observed and desorption of the ionic liquid sample was incomplete. These ionic liquids were the most viscous ionic liquids studied and consequently there was more ionic liquid present on the dipstick after each dip, as shown in Figure S2. For $[C_8C_1Im]Cl$ and $[C_8C_1Im]I$ a dip before every experiment was not necessary (as is the case for all other ionic liquids studied using LOSMS to date) as ionic liquid was normally present from the previous desorption experiment.

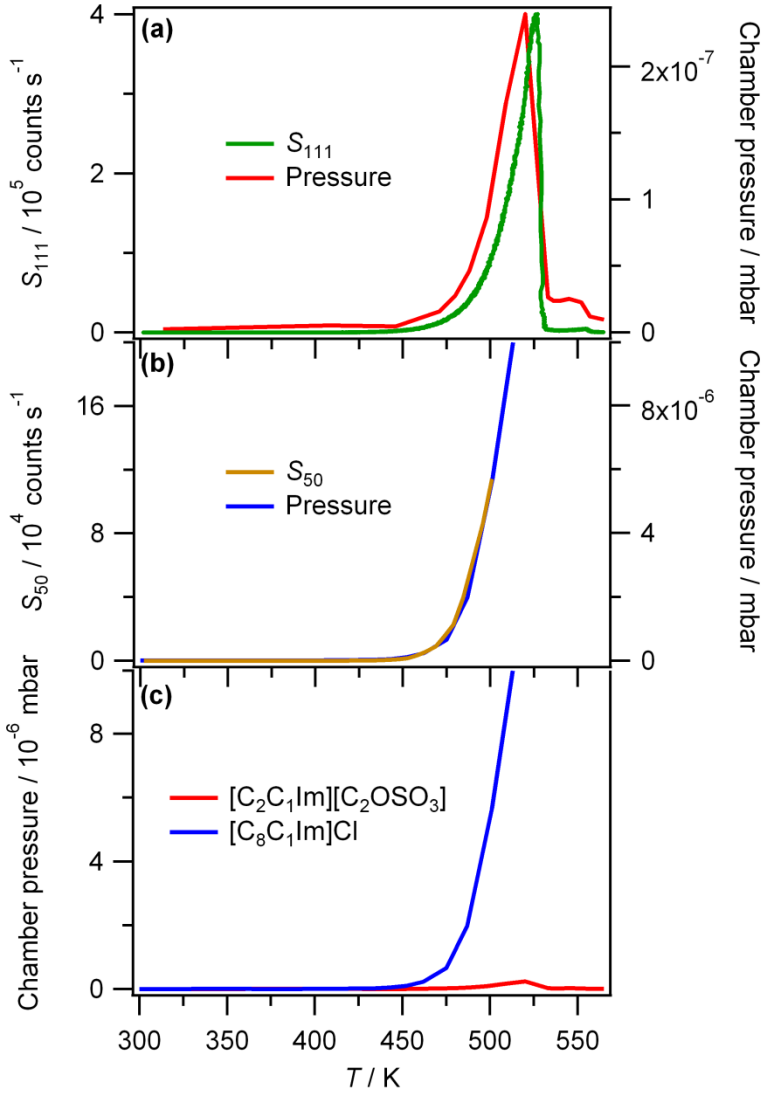

Figure S3. (a) Signal intensity for *m/z* 111, S_{50}, and ionisation gauge pressure *vs. T* for [C_2C_1Im][C_2OSO_3]. (b) Signal intensity for *m/z* 50, S_{50}, and ionisation gauge pressure *vs. T* for [C_8C_1Im]Cl. (c) Ionisation gauge pressure *vs. T* for [C_2C_1Im][C_2OSO_3] and [C_8C_1Im]Cl.

2. LOSMS set-up

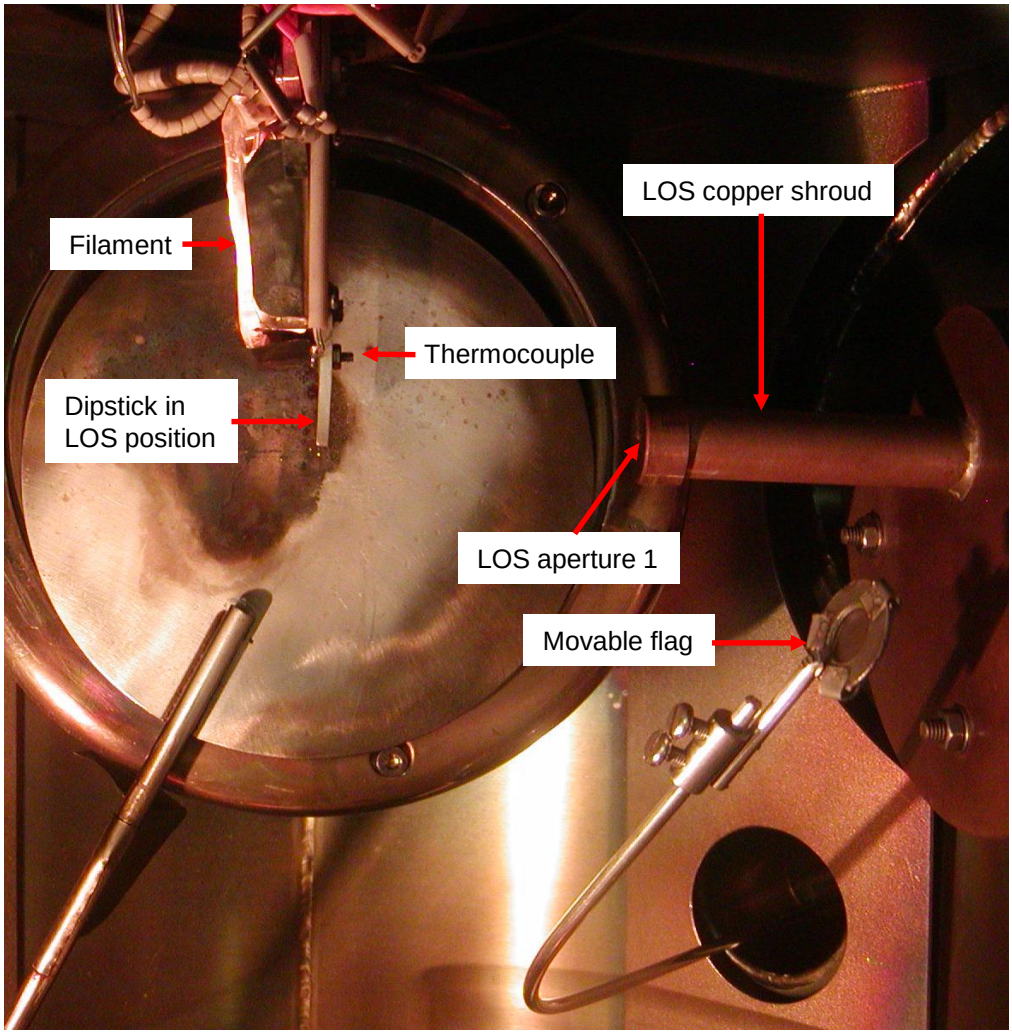

Figure S4. Annotated photograph of the LOSMS set-up. The sample heating filament was on when this photograph was taken.

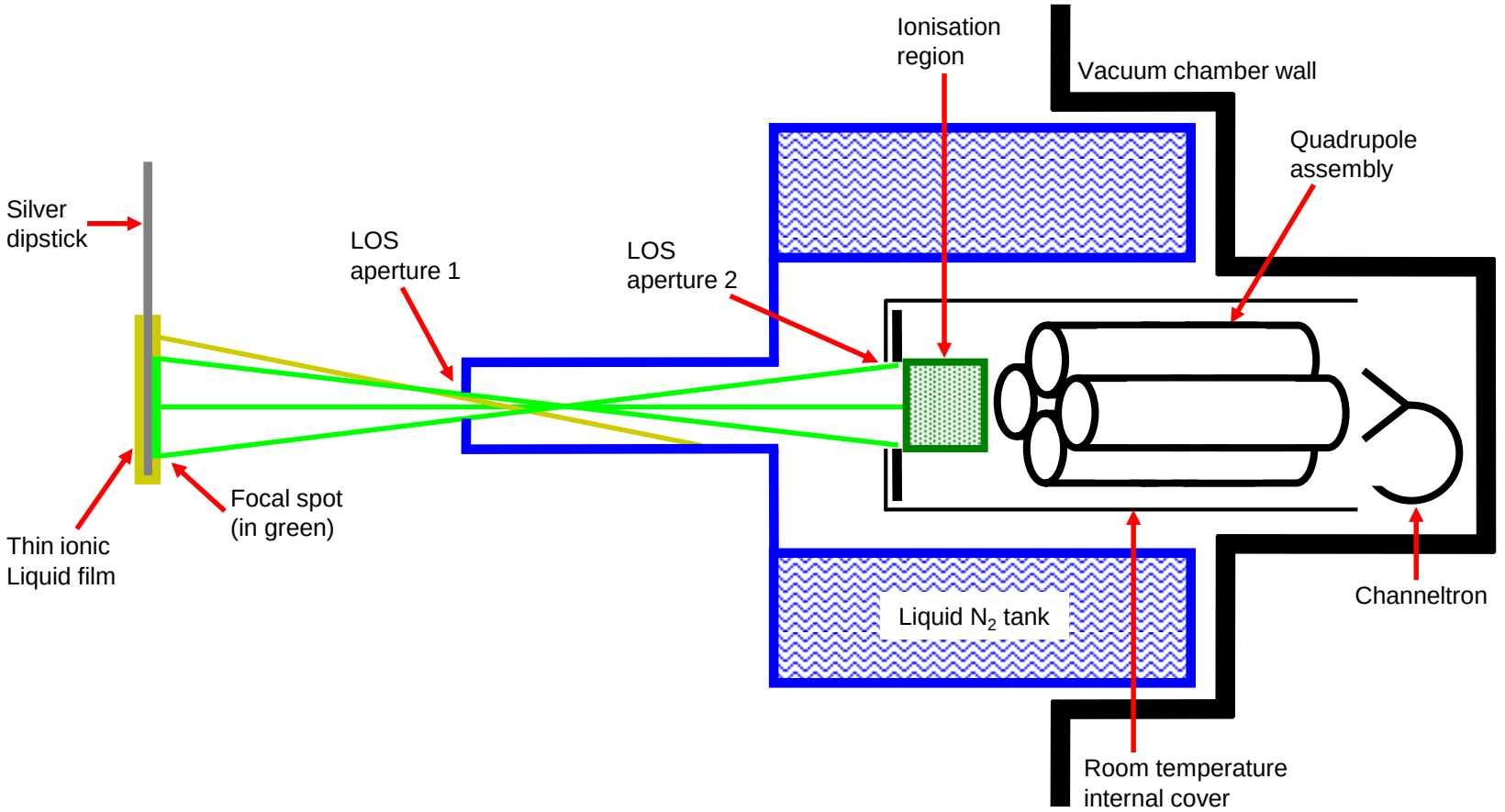

Figure S5. Schematic of LOS mass spectrometer (not to scale). Two LOS apertures define a focal spot on the surface of the sample, diameter ≈7 mm, in LOS with the ionisation region. The green species are in the field of view of the ionisation region; the yellow species are not.

3. Recording mass spectra

Due to the relatively low vapour density of the ionic liquid, a number of background gases present inside the mass spectrometer were observed; for example, *m/z* 28, $[CO]^{+\bullet}$, *m/z* 2, $[H_2]^{+\bullet}$, *m/z* 18, $[H_2O]^{+\bullet}$, *m/z* 44, $[CO_2]^{+\bullet}$. In addition, peaks due to mass spectrometer memory (peaks due to contaminants retained inside the mass spectrometer from previous experiments[1-7]) were observed. Normally a background subtraction would be employed; a background mass spectrum recorded before the desorption experiment began is subtracted from the vapour mass spectrum. However, it was found for these ionic liquid desorption experiments (where the heating rate is such that the temperature of interest is reached after approximately one hour of heating) that this procedure gave unsatisfactory background subtracted mass spectra, most likely due to the ionic liquid displacing relatively light molecules on the walls of the mass spectrometer and causing desorption. Therefore, a movable flag was used that can be manually placed in the LOS position between the ionisation volume and the dipstick. The ionic liquid vapour is therefore "blocked" from entering the mass spectrometer immediately before the "experimental" mass spectrum was recorded. This method gave satisfactory background subtracted mass spectra for ionic liquid vapour, as show in Figure S8 for $[C_8C_1Im]Cl$.

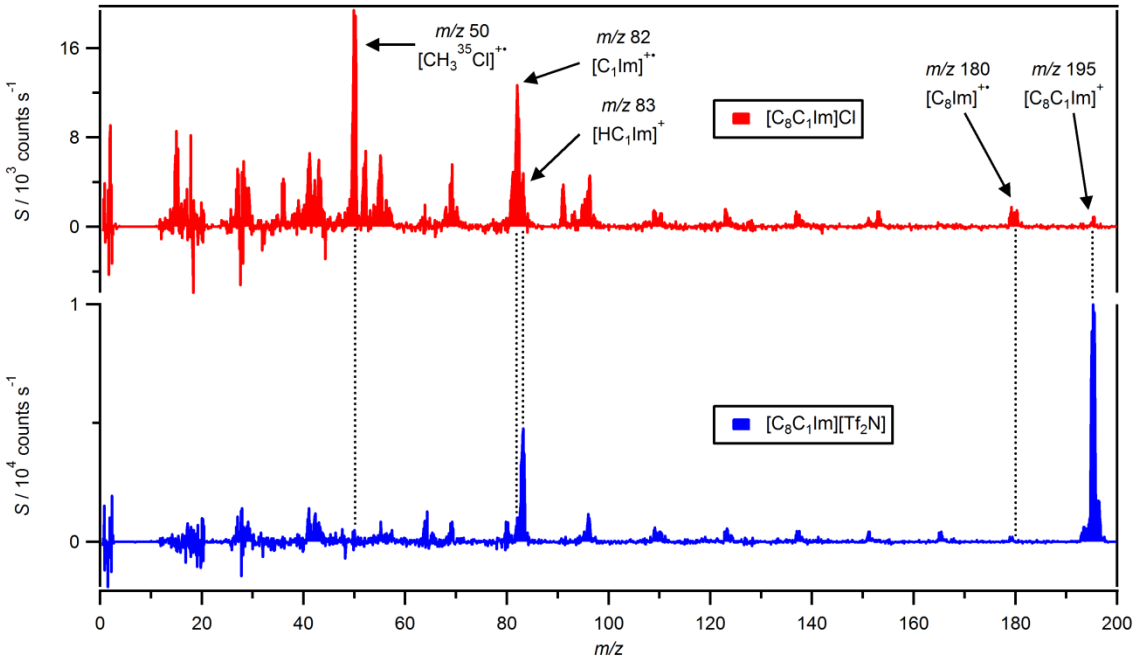

Figure S6. Background subtracted LOS mass spectrum signal intensity, *S*, versus *m/z* for: $[C_8C_1Im]Cl$ at 462 K and $[C_8C_1Im][Tf_2N]$ at 440 K.[6]

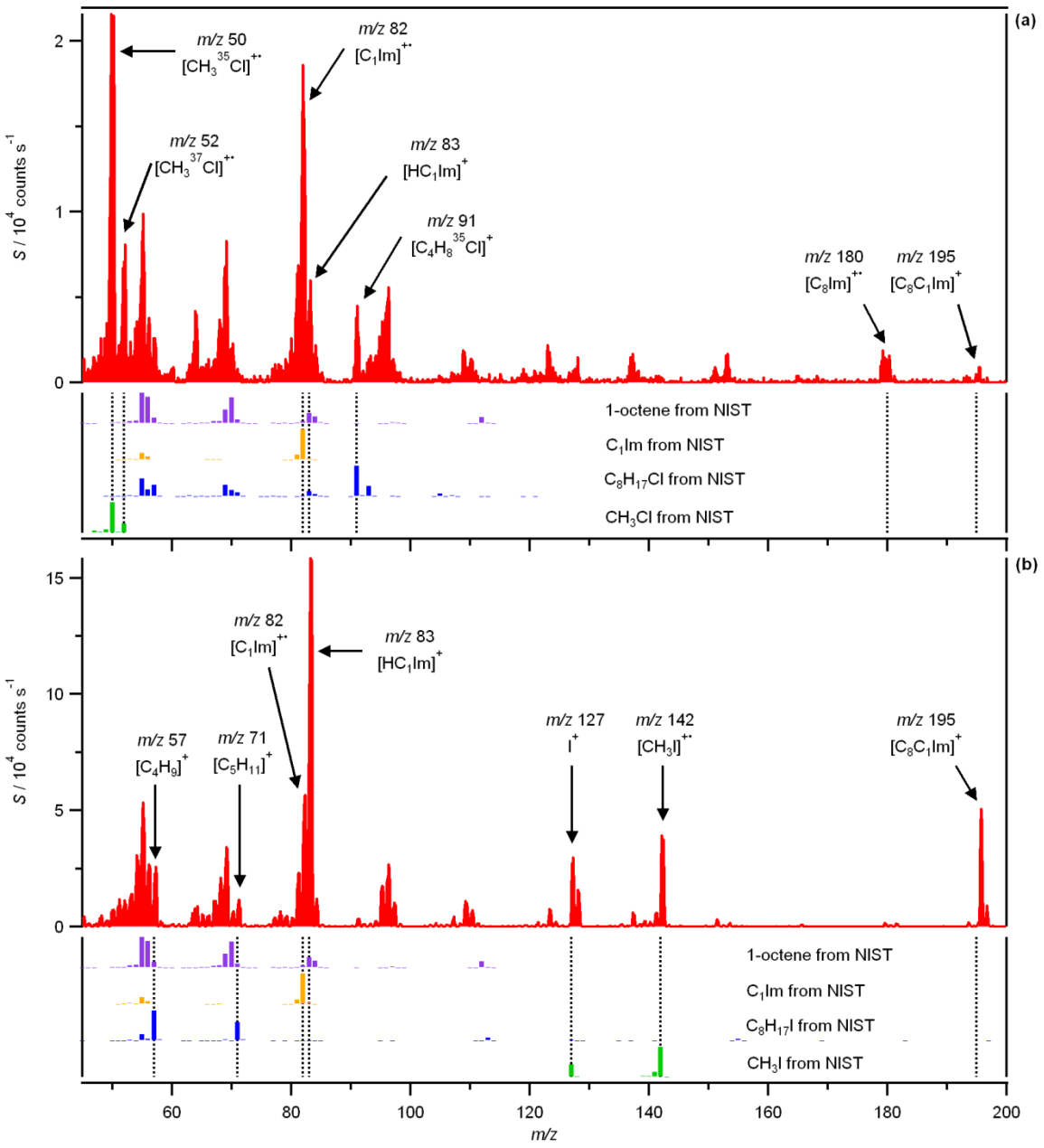

Figure S7. LOS mass spectrum signal intensity (not background subtracted), *S*, versus *m/z* for: (a) $[C_8C_1Im]Cl$ at 462 K, (b) $[C_8C_1Im]I$ at 532 K. For comparison purposes the mass spectra of 1-octene, methylchloride (CH_3Cl), 1-octylchloride ($C_8H_{17}Cl$), 1-methylimidazole (C_1Im), methyliodide (CH_3I) and 1-octyliodide ($C_8H_{17}I$).[8]

4. Low intensity of *m/z* 195 peak for $[C_8C_1Im]Cl$

The intensity of the *m/z* 195 peak for $[C_8C_1Im]Cl$ (Figure S8) is very low compared to the rest of the peaks. Is this low intensity due to a very low number density of NIPs in the vapour phase for $[C_8C_1Im]Cl$, or is it due to the fragmentation channels for the NIP after electron ionisation? To quantify the relative intensity of the *m/z* 195 peak, the peak signal intensity ratio for $[C_8C_1Im]^+$ to $[HC_1Im]^+$ is used. This ratio is ~0.3:1 for $[C_8C_1Im]Cl$ (using the data presented in Figure S8). The $[C_8C_1Im]^+$ to $[HC_1Im]^+$ ratio for $[C_8C_1Im][BF_4]$ is ~1.3:1;[6] the $[C_8C_1Im]^+$ to $[HC_1Im]^+$ ratio for $[C_8C_1Im][Tf_2N]$ is ~2.1:1.[6] Clearly, there is a trend in the $[C_8C_1Im]^+$ to $[HC_1Im]^+$ ratio: $[C_8C_1Im]Cl$ < $[C_8C_1Im][BF_4]$ < $[C_8C_1Im][Tf_2N]$. This trend follows the anion size (although a number of other quantities could be used to explain this trend for only four ionic liquids). Bearing in mind this trend, it is likely that the low intensity of the *m/z* 195 peak for $[C_8C_1Im]Cl$ is due to significant fragmentation of $[CA]^{+\bullet}$ to form products other than $[C_8C_1Im]^+$ rather than dominance in the vapour phase by the TPD products. One possible explanation for the trend is that larger anions, such as $[Tf_2N]^-$, are better at absorbing energy from the electron impact of electron ionisation. Hence, there is less energy transferred to $[C_8C_1Im]^+$ from electron impact, and therefore more $[C_8C_1Im]^+$ is observed relative to $[HC_1Im]^+$ for ionic liquids such as $[C_8C_1Im][Tf_2N]$ compared to $[C_8C_1Im]Cl$. More ionic liquids need to be studied with electron ionisation MS to give further insights into the fragmentation mechanisms.

5. Varying electron energy

The properties of $[C_8C_1Im]Cl$ NIPs were investigated further using LOSMS by measuring the ionisation energy, E_i; no measurements were made for $[C_8C_1Im]I$ NIPs. E_i is a measure of the energy required to remove the highest occupied molecular orbital (HOMO) electron. E_{app}, the appearance energy, for the parent cation is effectively the energy required to remove an electron from the ionic liquid NIP (*i.e.*, E_i) and dissociate the parent cation and the neutral radical, $E_{diss}(CA^{+\bullet})$. Hence:

$$E_{app}(C^+) = E_i(CA) + E_{diss}(CA^{+\bullet}) \quad (2)$$

As the molecular ion, $[CA]^{+\bullet}$, is not observed it is assumed that $E_{diss}(CA^{+\bullet})$ is negligible.

An electron ionisation efficiency curve for *m/z* 195, the parent cation $[C_8C_1Im]^+$, for $[C_8C_1Im]Cl$ is shown in Figure S6. For *m/z* 195, $[C_8C_1Im]^+$, no signal is observed below ~8 eV. From ~8 eV to 17 eV, an approximately linear relationship is observed between the signal for *m/z* 195 and the electron energy. From ~17 eV upwards, the signal gradually reaches a plateau (Figure S6 in the Supplementary Information). These observations suggest that there is only one mechanism for formation of $[C_8C_1Im]^+$ from $[C_8C_1Im]Cl$ NIPs, which is assumed to be dissociative ionisation of NIPs (Equation 1). We assume that $E_{app}(C^+) = E_i(CA)$, within the error of the experiment;[6, 9] by fitting a straight line to zero counts s^{-1} for the data in Figure S6a, for $[C_8C_1Im]Cl$ $E_i(CA)$ = 9.3 ± 0.4 eV was measured.

The number of ionic liquids is relatively small for which E_i for the NIP have been measured. In this contribution, $E_i(CA)$ for $[C_8C_1Im]Cl$ is measured as 9.3 ± 0.4 eV. $E_i(CA)$ for $[C_8C_1Im][Tf_2N]$ and $[C_8C_1Im][BF_4]$ are 11.2 ± 0.4 eV and 13.0 ± 0.4 eV respectively.[6] For $[C_8C_1Im][A]$, $E_i(CA)$ is Cl^- < $[Tf_2N]^-$ < $[BF_4]^-$. Literature $E_i(CA)$ values determined using photoionisation for $[C_2C_1Im][Tf_2N]$,

$[C_2C_1Im][(F_5C_2SO_2)_2N]$, $[C_3C_1C_1Im][Tf_2N]$ and $[C_4C_1Im][C(CN)_3]$ are 8.9 ± 0.2 eV, 9.0 ± 0.2 eV, 8.7 ± 0.35 eV and 6.6 ± 0.5 eV respectively (where $[C_3C_1C_1Im]^+$ = 1-propyl-2-methyl-3-methylimidazolium).[9-11] It is clear that more E_i(CA) values need to be measured for a sufficiently large range of ionic liquids for wide-ranging conclusions to be drawn.

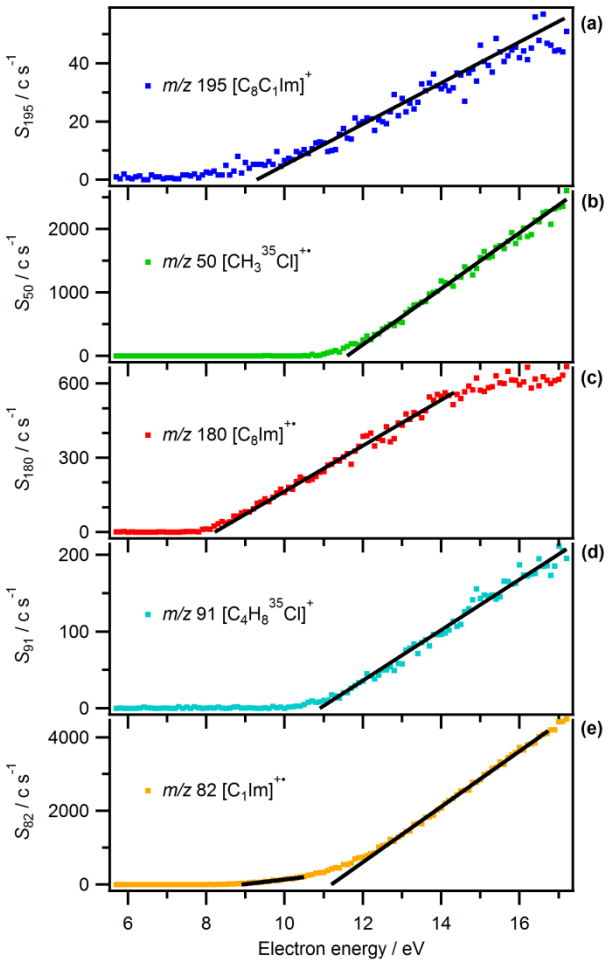

Figure S8. Electron ionisation efficiency curves close to the ionisation threshold for $[C_8C_1Im]Cl$ vapour for: (a) *m/z* 195, (b) *m/z* 50, (c) *m/z* 180, (d) *m/z* 91, (e) *m/z* 82. E_i and E_{app}, given in Table 3, are determined from where the solid straight lines cross zero counts s^{-1}. The experiments were performed at a sample temperature of 463 K.

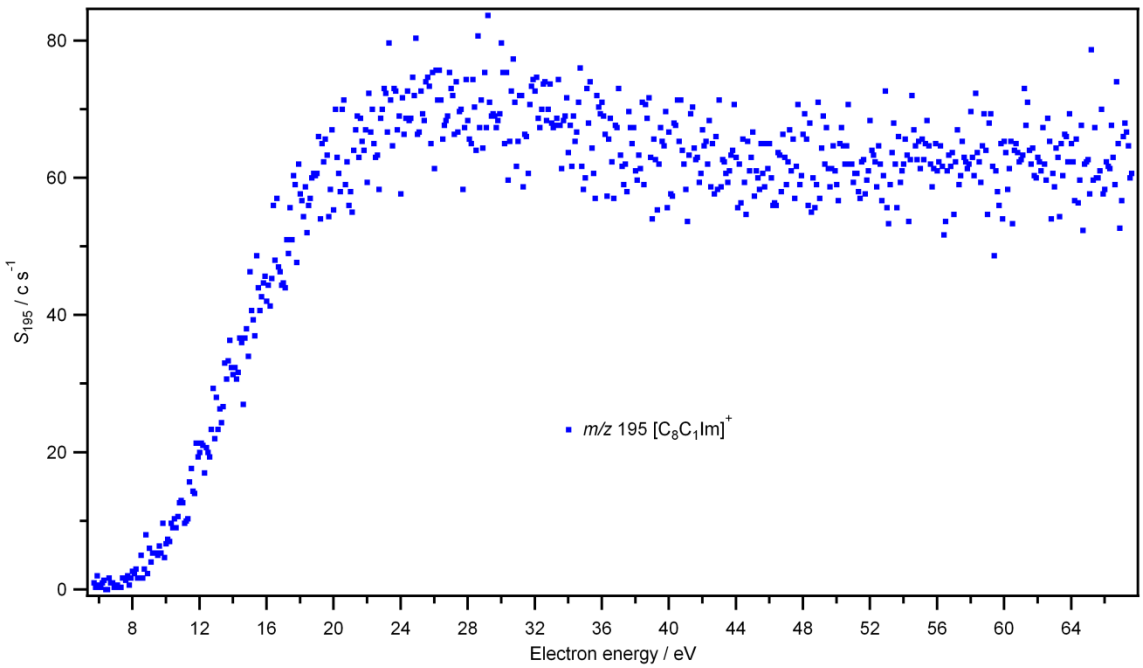

Figure S9. Electron ionisation efficiency curve for $[C_8C_1Im]Cl$ vapour for *m/z* 195. The experiment was performed at a sample temperature of 463 K.

6. Boiling points at atmospheric pressure and enthalpies of vaporisation for the TD products

Table S1. Boiling points at atmospheric pressure for the liquid phase TD products of $[C_8C_1Im]Cl$ and $[C_8C_1Im]I$.

Molecule	Nomenclature	Normal boiling point / K	$\Delta_{vap}H$ / kJ mol^{-1}
1-methylimidazole	C_1Im	471 [12]	
methylchloride	CH_3Cl	249 [13]	20.5 [14]
octylchloride	$C_8H_{17}Cl$	455 [15]	52.4 [16]
methyliodide	CH_3I	316 [17]	28.4 [18]
octyliodide	$C_8H_{17}I$	499 [15]	

7. Explaining TPD trace shape

The rate of NIP vaporisation is determined by the ionic liquid surface concentration within the area analysed by the LOS mass spectrometer. The area analysed by the LOS mass spectrometer is of course constant for all experiments, as demonstrated by the red spotted circles in Figure S10. From 300 K up to approximately 530 K, the bulk ionic liquid concentration varies a great deal, but ionic liquid surface concentration within the area analysed by the LOS mass spectrometer is essentially constant, as demonstrated by the front-on views of the dipstick in Figure S10. At ~530 K, there is a sharp decrease in *m/z* 195 signal intensity to zero counts s^{-1}. This intensity decrease is very rapid as the surface concentration suddenly changes from the value throughout the TPD experiment (300 K up to ~530 K) to a bare dipstick, *i.e.*, zero surface concentration (> ~550 K). These observations are indicative of zero order desorption of ionic liquid NIPs.

The rate of liquid phase TD is determined by the bulk ionic liquid concentration. The bulk ionic liquid concentration varies significantly during the TPD experiment due to both liquid phase TD and ionic liquid NIP vaporisation. This observation is demonstrated by the side-on views of the dipstick in Figure S10, where the ionic liquid film thickness clearly decreases as temperature increases. As the bulk ionic liquid concentration is not constant, desorption of liquid phase TD products does not follow zero order kinetics. The rate of liquid phase TD is determined by the bulk ionic liquid concentration and is likely to follow either 1^{st} or 2^{nd} order kinetics. The bulk ionic liquid concentration decreases due to both liquid phase TD and ionic liquid NIP vaporisation. From the results given here we are unable to determine the order of liquid phase TD.

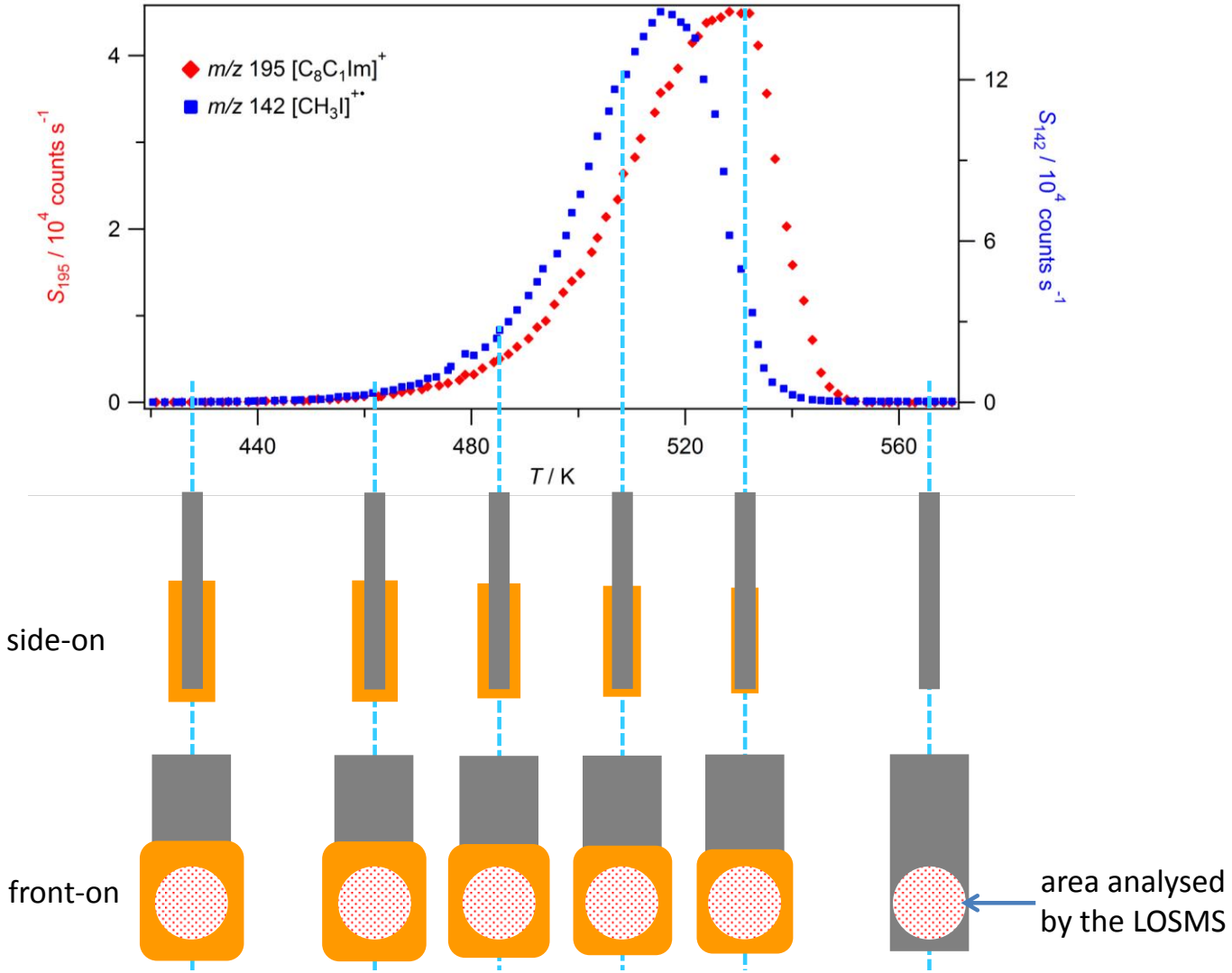

Figure S10. LOS mass spectrum signal intensity, *S*, versus temperature, *T*, for $[C_8C_1Im]I$ between 420 K and 570 K for *m/z* 195, $[C_8C_1Im]^+$, and *m/z* 142, $[CH_3I]^{+\bullet}$. The side-on and front-on schematic views of the ionic liquid on the dipstick are given to explain how the ionic liquid surface concentration is constant throughout most of the TPD experiment, whereas the bulk ionic liquid concentration varies throughout most of the TPD experiment.

References

1. J. P. Armstrong, C. Hurst, R. G. Jones, P. Licence, K. R. J. Lovelock, C. J. Satterley and I. J. Villar-Garcia, *Phys. Chem. Chem. Phys.*, 2007, **9**, 982-990.
2. V. N. Emel'yanenko, S. P. Verevkin, A. Heintz, J. A. Corfield, A. Deyko, K. R. J. Lovelock, P. Licence and R. G. Jones, *J. Phys. Chem. B*, 2008, **112**, 11734-11742.
3. A. Deyko, K. R. J. Lovelock, J. A. Corfield, A. W. Taylor, P. N. Gooden, I. J. Villar-Garcia, P. Licence, R. G. Jones, V. G. Krasovskiy, E. A. Chernikova and L. M. Kustov, *Phys. Chem. Chem. Phys.*, 2009, **11**, 8544-8555.
4. K. R. J. Lovelock, A. Deyko, J. A. Corfield, P. N. Gooden, P. Licence and R. G. Jones, *ChemPhysChem*, 2009, **10**, 337-340.
5. K. R. J. Lovelock, A. Deyko, P. Licence and R. G. Jones, *Phys. Chem. Chem. Phys.*, 2010, **12**, 8893-8901.
6. A. Deyko, K. R. J. Lovelock, P. Licence and R. G. Jones, *Phys. Chem. Chem. Phys.*, 2011, **13**, 16841-16850.
7. A. Deyko, S. G. Hessey, P. Licence, E. A. Chernikova, V. G. Krasovskiy, L. M. Kustov and R. G. Jones, *Phys. Chem. Chem. Phys.*, 2012, **14**, 3181-3193.
8. S. E. Stein, *"Mass Spectra" in NIST Chemistry WebBook, NIST Standard Reference Database Number 69*, National Institute of Standards and Technology, Gaithersburg 2005.
9. D. Strasser, F. Goulay, L. Belau, O. Kostko, C. Koh, S. D. Chambreau, G. L. Vaghjiani, M. Ahmed and S. R. Leone, *J. Phys. Chem. A*, 2010, **114**, 879-883.
10. D. Strasser, F. Goulay, M. S. Kelkar, E. J. Maginn and S. R. Leone, *J. Phys. Chem. A*, 2007, **111**, 3191-3195.
11. S. D. Chambreau, G. L. Vaghjiani, C. J. Koh, A. Golan and S. R. Leone, *J. Phys. Chem. Lett.*, 2012, **3**, 2910-2914.
12. *Catalog Handbook of Fine Chemicals*, Aldrich Chemical Company Inc., Milwaukee, 1990.
13. J. F. Norris and B. M. Sturgis, 1939, **61**, 1413-1417.
14. J. A. Manion, *J. Phys. Chem. Ref. Data*, 2002, **31**, 123-172.
15. D. R. Lide, ed., *Handbook Chemistry and Physics: a ready-reference book of chemical and physical data*, 87th edn., CRC Press, Boca Raton, 2006.
16. V. Majer and V. Svoboda, *Enthalpies of Vaporization of Organic Compounds: A Critical Review and Data Compilation*, Blackwell Scientific Publications, Oxford, 1985.
17. F. V. Grimm and W. A. Patrick, 1923, **45**, 2794–2802.
18. H. W. Thompson and J. W. Linnett, *Trans. Faraday Soc*, 1936, **32**, 681-685.